30. Schulze-Makuch, D. & Grinspoon, D. H. Biologically enhanced energy and carbon cycling on Titan. *Astrobiology* **5**(4), 560–567 (2005).

Supplementary Information is linked to the online version of the paper at www.nature.com/nature.

Acknowledgements The Cassini-Huygens mission is the result of an exemplary international collaboration in space exploration. Huygens involved more than 40 European industries and two US suppliers. The work of the members of the Cassini and Huygens teams from ESA, NASA/JPL, the Huygens industrial consortium led by Alcatel, and all Cassini-Huygens investigators is acknowledged. We especially acknowledge the Cassini orbiter teams that made their early observations available in advance to Huygens, and to R. Yelle for his leadership in coordinating the Titan Atmosphere Model Working Group. Special acknowledgements to B. Smeds for his work in designing and managing the Huygens link test that allowed the Doppler problem to be detected and solved, to L. Popken for his modelling of the Huygens Digital Radio Receiver and to the whole Huygens recovery task force led by K. Clausen and L. Deutsch. We thank K. van't Klooster for his efforts to initiate and promote the Huygens VLBI experiment, and J. Louet for his support. The Earth-Based Huygens Doppler tracking experiment is led by W. Folkner. We appreciated the support provided by the National Radio Astronomy Observatory (NRAO), operated by Associated Universities Inc., under a cooperative agreement with the NSF, and the one provided by the Australia Telescope National Facility (ATNF) managed by CSIRO. We also thank M. Bird, R. Lorenz, R. A. Preston and J. C. Zarnecki for a careful reading of various versions of the manuscript and for providing comments.

Author Information Reprints and permissions information is available at npg.nature.com/reprintsandpermissions. The authors declare no competing financial interests. Correspondence and requests for materials should be addressed to J.-P.L. (jean-pierre.lebreton@esa.int).

ARTICLES

Rain, winds and haze during the Huygens probe's descent to Titan's surface

M. G. Tomasko[1], B. Archinal[2], T. Becker[2], B. Bézard[3], M. Bushroe[1], M. Combes[3], D. Cook[2], A. Coustenis[3], C. de Bergh[3], L. E. Dafoe[1], L. Doose[1], S. Douté[4], A. Eibl[1], S. Engel[1], F. Gliem[5], B. Grieger[6], K. Holso[1], E. Howington-Kraus[2], E. Karkoschka[1], H. U. Keller[6], R. Kirk[2], R. Kramm[6], M. Küppers[6], P. Lanagan[1], E. Lellouch[3], M. Lemmon[7], J. Lunine[1,8], E. McFarlane[1], J. Moores[1], G. M. Prout[1], B. Rizk[1], M. Rosiek[2], P. Rueffer[5], S. E. Schröder[6], B. Schmitt[4], C. See[1], P. Smith[1], L. Soderblom[2], N. Thomas[9] & R. West[10]

The irreversible conversion of methane into higher hydrocarbons in Titan's stratosphere implies a surface or subsurface methane reservoir. Recent measurements from the cameras aboard the Cassini orbiter fail to see a global reservoir, but the methane and smog in Titan's atmosphere impedes the search for hydrocarbons on the surface. Here we report spectra and high-resolution images obtained by the Huygens Probe Descent Imager/Spectral Radiometer instrument in Titan's atmosphere. Although these images do not show liquid hydrocarbon pools on the surface, they do reveal the traces of once flowing liquid. Surprisingly like Earth, the brighter highland regions show complex systems draining into flat, dark lowlands. Images taken after landing are of a dry riverbed. The infrared reflectance spectrum measured for the surface is unlike any other in the Solar System; there is a red slope in the optical range that is consistent with an organic material such as tholins, and absorption from water ice is seen. However, a blue slope in the near-infrared suggests another, unknown constituent. The number density of haze particles increases by a factor of just a few from an altitude of 150 km to the surface, with no clear space below the tropopause. The methane relative humidity near the surface is 50 per cent.

The surface of Titan has long been studied with various instruments, including those on the Hubble Space Telescope (HST) and ground-based adaptive optics systems[1]. More recently, Cassini investigations using the charge-coupled device (CCD) camera[2], the Visible and Infrared Mapping Spectrometer (VIMS) instrument[3], and the Radio Detection and Ranging (RADAR) imaging system[4] have provided more detailed views of Titan's surface in the hope of revealing how the methane in Titan's atmosphere is replenished from the surface or interior of Titan. Of the Cassini imagers, the Imaging Science Subsystem (ISS) camera is potentially capable of the greatest spatial resolution, but Titan's obscuring haze limits its resolution on the surface to about 1 km, a value roughly similar to that available from VIMS and the radar imaging system. At this resolution, the bright and dark regions observed on the surface of Titan have proved difficult to interpret. Owing to its proximity to the surface, the Descent Imager/Spectral Radiometer (DISR) camera on the Huygens probe was capable of a linear resolution of some metres from a height of 10 km. In addition, the lower the probe descended, the less haze lay between the camera and the ground. The DISR was capable of linear resolution orders of magnitude better than has been available from orbit, although of a much smaller portion of Titan's surface. Also, a lamp was used at low altitude to measure the continuous reflectance spectrum of the surface without the complications introduced by observations through large amounts of methane and aerosol haze[5].

In addition to studying the surface of Titan, the DISR took measurements of solar radiation in the atmosphere. Spectrometers looking upward at continuum wavelengths (between the major methane absorptions) as well as downward measured the vertical distribution and wavelength dependence of the aerosol haze opacity. Measurements of the polarization of light at a scattering angle of 90° constrained the small dimension of the haze particles. Measurements of the brightness in the solar aureole around the Sun determined the projected area of the haze particles. Observations in the methane bands determined the methane mole fraction profile.

Data collection during the descent proceeded mostly, although not exactly, as planned. Turbulence during the first half of the descent tipped the probe more rapidly than expected, causing the Sun sensor to remain locked on the azimuth of the Sun for only a few successive rotations at a time. Below about 35 km, the signal from the direct solar beam was lost by the Sun sensor owing to the unexpectedly low temperature of this detector. These effects caused data from each of the DISR sub-instruments to be collected at mostly random, instead of specific, azimuths. Additionally, the probe rotated in the intended direction for only the first ten minutes before rotating in the opposite sense for the remainder of the descent. This resulted in ineffective baffling of the direct solar beam for the upward-looking visible spectrometer and the solar aureole camera. Consequently, some measurements made by the solar aureole camera are saturated, and the separation of the direct and diffuse solar beams in the visible spectral measurements must be postponed until a good model of the probe attitude versus time is available. Finally, the loss of one of

[1]Lunar and Planetary Laboratory, University of Arizona, 1629 E. University Blvd, Tucson, Arizona 85721-0092, USA. [2]US Geological Survey, Astrogeology, 2225 N. Gemini Drive, Flagstaff, Arizona 86001, USA. [3]LESIA, Observatoire de Paris, 5 place Janssen, 92195 Meudon, France. [4]Laboratoire de Planétologie de Grenoble, CNRS-UJF, BP 53, 38041 Grenoble, France. [5]Technical University of Braunschweig, Hans-Sommer-Str. 66, D-38106 Braunschweig, Germany. [6]Max Planck Institute for Solar System Research, Max-Planck-Str. 2, D-37191 Katlenburg-Lindau, Germany. [7]Department of Physics, Texas A&M University, College Station, Texas 77843-3150, USA. [8]Istituto Nazionale di Astrofisica – Istituto di Fisica dello Spazio Interplanetario (INAF-IFSI ARTOV), Via del Cavaliere, 100, 00133 Roma, Italia. [9]Department of Physics, University of Bern, Sidlerstr. 5, CH-3012 Bern, Switzerland. [10]Jet Propulsion Laboratory, 4800 Oak Grove Drive, Pasadena, California 91109, USA.

the two radio communication channels in the probe receiver aboard the orbiter resulted in the loss of half the images as well as several other low-altitude spectrometer measurements.

Despite these misfortunes, the DISR instrument collected a unique and very useful data set. Images of the surface with unprecedented resolution were collected over the boundary between bright and dark terrain seen from the orbiter. Owing to redundant transmission over both communication channels during most of the descent, almost all of the spectral and solar aureole observations were received. A very large set of high-quality spectra were obtained with good altitude resolution and with good coverage in azimuth both away from and towards the Sun. The images, the spectra, the Sun sensor pulses, the recording of the gain in the Cassini radio receiver, and information from Very Long Baseline Interferometry (VLBI) observations from Earth together will permit reconstruction of the probe attitude relative to the Sun as a function of time during the descent, enabling a full analysis of the spectral data. The large number of solar aureole measurements included several acquired near the Sun and many polarization measurements opposite to the Sun. The surface science lamp worked exactly as planned, permitting surface reflection measurements even in strong methane absorption bands. Operations after landing included the collection of successive images as well as spectral reflectance measurements of the surface illuminated by the lamp from an assumed height of roughly 30 cm.

Taken together, the new observations shed substantial light on the role played by methane in forming the surface of Titan and how it is recycled into the atmosphere. The substantial relative humidity of methane at the surface and the obvious evidence of fluid flow on the surface provide evidence for precipitation of methane onto the surface and subsequent evaporation. Some indications of cryovolcanic flows are also seen. The vertical distribution and optical properties of Titan's haze have been characterized to aid the interpretation of remote measurements of the spectral reflection of the surface. The speed and direction of Titan's winds has also been measured for comparison with future dynamical models that include the radiative heating and cooling rates implied by the haze.

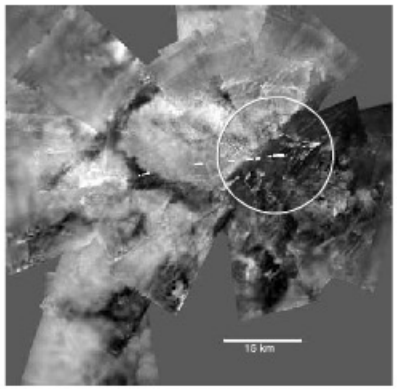

Figure 1 | View of Titan from 34 km above its surface. High-altitude (49 to 20 km) panoramic mosaic constructed from the DISR High and Medium Resolution Imagers (HRI and MRI) as projected from 34 km. The preliminary ground-track solution (indicated as small white points on gnomonic ground projection) represents the location of the probe when data were collected; north points up; scale indicated (although subsequent analysis indicates that north lies some 5–10° to the left of straight up in this and the two subsequent figures). Starting from the first surface image at 49 km, the probe moves in an east-northeastwardly direction at an initial speed of 20 m s^{-1}. Brighter regions separated by lanes or lineaments of darker material are seen. No obvious crater-like features are visible. The circle indicates the outline of the next-lowest pan, in Fig. 2. The method used for construction of panoramic mosaics incorporates knowledge of the probe's spatial location (longitude, latitude and altitude) and attitude (roll, pitch and yaw) at each image. With the exception of altitude, provided by the Huygens Atmospheric Structure Instrument[11] pressure sensor, none of these variables was directly measured. They are found through an iterative process in which a panorama is created, providing an improved ground-track and azimuth model, which results in an upgraded trajectory, which can improve the panorama, and so on. The current lack of pitch and roll knowledge constitutes the main source of error in the current composition and quality of the panoramas as well as the ground-track and wind speed determination reported below. Vigorous contrast-stretching in the images is required to reveal details washed out by the haze particle density at all altitudes in Titan's atmosphere. This contrast-stretching also displays the occasional ringing of the Discrete Cosine Transform data compressor, which appear as regular lines of bright and dark patterns, particularly in the MRI images.

Physical processes that form the surface

The imagers provided views of Titan's previously unseen surface, thus allowing a deeper understanding of the moon's geology. The three DISR cameras were designed to provide overlapping coverage for an unbroken 360°-wide swath stretching from nadir angles between 6° and 96°. Some 20 sets of such images were planned during the descent. Because of the opacity of the haze in the passband of our imager, surface features could be discerned in the images only below about 50 km, limiting the number of independent panoramic mosaics that can be made of the surface. The loss of half of the images meant that Titan's surface was not covered by systematic overlapping triplets, as expected. Three different views of Titan's surface are shown in Figs 1 to 3. A view of Titan's surface after the Huygens landing is shown in Fig. 4.

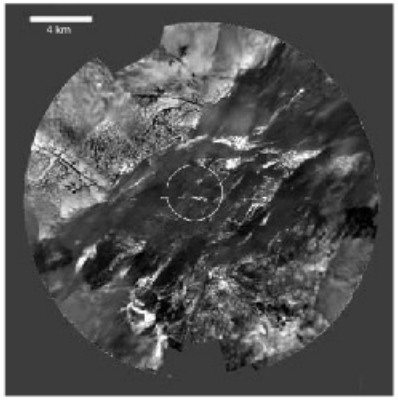

Figure 2 | View from 8 km. Medium-altitude (17 to 8 km) panoramic mosaic projected from 8 km. As in Fig. 1, the preliminary ground-track solution is indicated as points; north is up; scale indicated. At 11 km, the wind direction is at 0° (eastward), reaching −20° (southeastward) at an altitude of 8.5 km. The narrow dark lineaments, interpreted as channels, cut brighter terrain. The circle indicates the outline of the low-altitude pan in Fig. 3.

The highest view (Fig. 1), projected from an altitude of 34 km, displays an albedo variation very similar to the highest-resolution images provided by the ISS or VIMS cameras on the Cassini orbiter. It shows Titan's surface to consist of brighter regions separated by lanes or lineaments of darker material. No obvious impact features are visible, although craters less than roughly 10 km should not be abundant as a result of atmospheric shielding[6]. In the rightmost (eastern) part of the mosaic the images become sharper as the lower altitude of the camera causes the scale to decrease and the contrast to increase. More than a dozen brighter areas in that region seem to be elongated along a direction parallel with the main bright/dark boundary of that region. At the limit of resolution, narrow dark channels cut the bright terrain.

The next view, Fig. 2, projected from an altitude of 8 km, reveals a large number of these channels (detailed in Fig. 5). The channel networks have two distinct patterns: short stubby features and dendritic features with many branches. The region of the stubby network towards the west is significantly brighter than the dendritic region. The stubby channels are shorter, wider and relatively straight. They are associated with and often begin or end in dark circular areas, which suggest ponds or perhaps pits. The morphology of rectilinear networks with stubby heads is consistent with spring-fed channels or arroyos.

The dendritic network is consistent with rainfall drainage channels, implying a distributed rather than a localized source of a low-viscosity liquid. Stereo analysis of the dendritic region indicates an elevation of 50–200 m relative to the large darker plain to the south. It suggests that the brighter areas within the darker terrain are higher as well. The topographic differences are evident in Figs 6 and 7, which are three-dimensional renderings of the area just north of the landing site produced from the DISR images. They include the major bright–dark interface seen from above in Fig. 5. Figure 2 depicts many examples of these darker lanes of material between topographically higher, brighter areas. In fact the low contrast of the lowland plane argues that the entire dark region floods, and as the liquid drains the local topography drives flows as seen in the images. If the darker region is interpreted as a dried lakebed, it is too large to have been caused by the creeks and channels visible in the images. It may have been created by other larger river systems or some large-scale catastrophic event, which predates deposition by the rivers seen in these images.

The interpretation of the dark lanes within the brighter highlands as drainage features is so compelling as to dominate subsequent interpretation of other areas of images such as Figs 2 and 3. The prevailing bright–dark boundary of the region becomes a coastline, the bright areas separated from this boundary become islands. Bright streaks running parallel to the albedo boundary may be drift deposits or splays fractured off the bright highlands owing to faulting along the shoreline.

When coupled with Fig. 4, which is an image of a typical offshore dark region, it is clear that the analogy has a limit. At present there is no liquid in the large dark lakebed imaged in Figs 1 to 5. The bright lobate feature, split by an apparently straight dark lane in the western part of the mosaic in Fig. 2, is a possible fissure-fed cryovolcanic flow. However, Fig. 4 also reveals rocks which—whether made of silicates or, more probably hydrocarbon-coated water-ice—appear to be rounded, size-selected and size-layered as though located in the bed of a stream within the large dark lakebed. Rounded stones approximately 15 cm in diameter and probably composed of water-ice, lie on top of a darker, finer-grained surface.

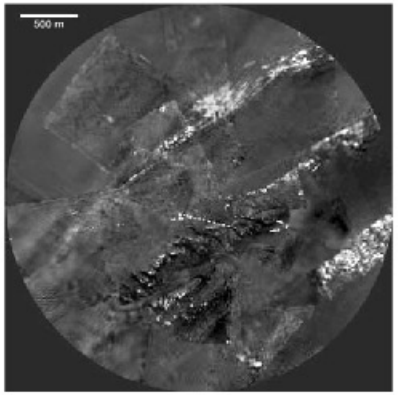

Figure 3 | View from 1.2 km. Low-altitude (7 to 0.5 km) panoramic mosaic projected from 1,200 m. As in Figs 1 and 2, the preliminary ground track is indicated as points; north is up; scale indicated. The probe's steady east-northeast drift halts altogether at an altitude of 7 km and reverses, moving west-northwest for some 1 km during the last 15 min of descent. Note the ridge near the centre, cut by a dozen darker lanes or channels. The projected landing site is marked with an 'X' near the continuation of one of the channels, whose direction matches the orientation of the stream-like clearing in the near-foreground of the southward-looking surface image, Fig. 4.

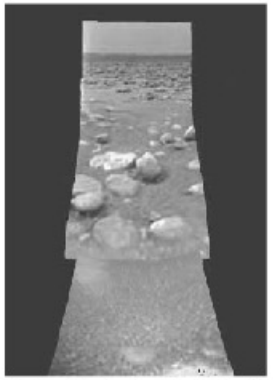

Figure 4 | The view from Titan's surface. Merged MRI and SLI images acquired after the Huygens probe soft-landing. Horizon position implies a pitch of the DISR nose upward by 1.7 ± 0.2° with no measurable roll. 'Stones' 10–15 cm in size lie above darker, finer-grained substrate in a variable spatial distribution. Brightening of the upper left side of several rocks suggests solar illumination from that direction, implying a southerly view, which agrees with preliminary evidence from other data sets. A region with a relatively low number of rocks lies between clusters of rocks in the foreground and the background and matches the general orientation of channel-like features in the low-altitude pan of Fig. 3. The bright spot in the lower right corner is the illumination of the DISR surface science lamp.

It is interesting to compare the brightness and colour of the scene shown in Fig. 4 with that of a similar scene on the Earth. The brightness of the surface of the Earth illuminated by full sunlight is about half a million times greater than when illuminated by a full moon. The brightness of the surface of Titan is about a thousand times dimmer than full solar illumination on the Earth (or 500 times brighter than illumination by full moonlight). That is, the illumination level is about that experienced about 10 min after sunset on the Earth. The colour of the sky and the scene on Titan is rather orange due to the much greater attenuation of blue light by Titan's haze relative to red light. If the Sun is high in the sky, it is visible as a small, bright spot, ten times smaller than the solar disk seen from Earth, comparable in size and brightness to a car headlight seen from about 150 m away. The Sun casts sharp shadows, but of low contrast, because some 90% of the illumination comes from the sky. If the Sun is low in the sky, it is not visible.

The sizes of the more than 50 stones in the image in Fig. 4 vary between 3 mm in diameter, the resolution limit of the imager, and 15 cm. No rocks larger than 15 cm are seen. The resolution of the last images taken before landing from a height of 200–300 m would be sufficient to identify metre-sized objects, and none are seen in the 40 × 35 m field of view. Figure 8 shows the *R* value, a measure of the fraction of the surface covered by rocks of a given size frequently used to describe the size distribution of impact craters or crater ejecta. A larger fraction of the surface is covered with rocks greater than 5 cm as opposed to smaller pebbles. The dominance of the cobbles 5–15 cm in size suggests that rocks larger than ~15 cm cannot be transported to the lakebed, while small pebbles (<5 cm) are quickly removed from the surface. Figure 8 confirms the visual impression given by Fig. 4 that the surface coverage of rocks in the foreground of the image (<80 cm horizontal distance from the probe) is higher than in the region beyond (about 80–160 cm). However, this trend is not seen for the pebbles less than 5 cm in size.

Elongated dark trails aligned with the general trend of the possible stream-bed visible in the centre of Fig. 4 extend from several of the distant boulders. The direction of the trails agrees with the general northwest–southeast alignment of the stream-like features shown in Fig. 3, because the last upward-looking spectra indicate that the probe settled with DISR facing southward. Images taken from the surface show no traces of the landing of the probe. The viewing direction is probably generally not downwind (the parachute is not visible).

When coupled with the shapes, size selection and layering of the stones in Fig. 4, the elongated islands and their orientation parallel to the coastline in Fig. 1, the stubby and dendritic channel networks, as well as the ponds in Fig. 2 and Fig. 5, the major elements of the Titan surface albedo variations can be interpreted to be controlled by flow of low-viscosity fluids driven by topographic variation, whether caused by precipitation (the dendritic networks) or spring-fed flows (the stubby networks). We thus interpret the bright–dark albedo difference as follows: irrigation of the bright terrain results in darker material being removed and carried into the channels, which discharge it into the region offshore, thereby darkening it. Eolian processes such as wind gusts coupled with Titan's low gravity (compared to Earth) may aid this migration.

The dark channels visible in the lowest panorama (Fig. 3) seem to suggest south-easterly fluid flow across the lower plane, depositing or exposing the brighter materials (water ice[6]) along the upstream faces of the ridges.

Stereographic rendering of the dendritic channels just north of the probe landing site (Figs 6 and 7) shows that the slopes in bright terrain being dissected by the putative methane river channels are extremely rugged; slopes of the order of 30° are common. This suggests relatively rapid erosion by flows in the river beds, resulting in the deeply incised valleys. Erosion by steep landslides on slopes approaching the angle of repose is probably the primary mechanism by which the rugged topography is formed. Figure 7 shows two stereographic views of the shoreline and hillside north of the landing site.

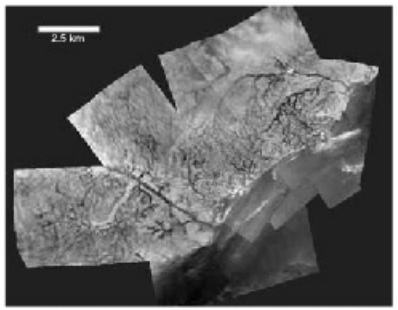

Figure 5 | View of 'shoreline' and channels. Panoramic mosaic projected from 6.5 km, showing expanded view of the highlands and bright–dark interface. As in previous figures, north is up; scale indicated. Branching and rectilinear channel networks of dark lanes are shown along an albedo boundary approximately 12 km long.

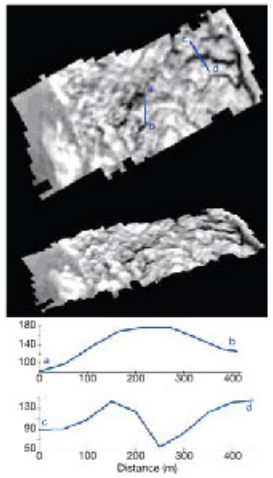

Figure 6 | Topographic model of highland region ~5 km north of the Huygens landing site. The top panel shows an orthorectified HRI image from stereo pair (vertical view). The middle panel shows a perspective view of the topographic model with ~50° tilt angle. No vertical exaggeration was applied (it is 1:1). The bottom panel shows profiles (a–b and c–d from the top panel) that illustrate the extremely steep topography in the region dissected by the drainages. All dimensions are in metres. A DISR stereo pair (using HRI frame 450 and MRI frame 601) was photogrammetrically analysed using a digital stereo workstation. The overlapping area of stereo coverage is about 1 × 3 km; the convergence angle is ~25°. The coincidence of the drainage patterns with the valley floors gives confidence in the reality of the topographic model; the height accuracy is ~20 m. This preliminary model has been arbitrarily levelled so that the elevation differences are only relative.

The wind profile

Assembly of the panoramic mosaics leads to the construction of a descent trajectory as part of an iterative process of image reconstruction. The trajectory can be used to derive the probe ground track and extract the implied wind velocity as a function of altitude. Correlation of the roughly 200 usable images acquired by DISR during its descent resulted in longitude and latitude values versus time, displayed in Fig. 9. Fitted by polynomials, these ground tracks were differentiated with respect to time and scaled to derive the horizontal wind speed and direction as functions of altitude.

The results indicate that the probe's steadily increasing eastward drift caused by Titan's prograde winds, as shown in Fig. 10, slowed from near 30 to 10 m s^{-1} between altitudes of 50 and 30 km and slowed more rapidly (from 10 to 4 m s^{-1}) between altitudes of 30 and 20 km. The winds drop to zero and reverse at around 7 km, near the expected top of the planetary boundary layer, producing a west-northwestwardly motion extending for about 1 km during the last 15 min of the descent (see Fig. 3). The generally prograde nature of the winds between 50 and 10 km agrees with models of Titan's zonal winds available before the arrival of Cassini or the Huygens probe[7], although the wind speed is somewhat less than the average predicted before entry.

The planetary boundary layer is calculated to have a thickness of between 4 and 8 km, based on scaling the Earth's near-equatorial planetary-boundary-layer thickness of 1–2 km by the inverse square-rooted ratio of the planetary rotation rates. The minimum horizontal wind speed at 7 km can thus be an indication of entry into the boundary layer[8]. The reversal of wind direction at this altitude is also consistent with the Voyager-derived equatorial temperature profile[9], wherein the temperature gradient changes from dry adiabatic to a sub-adiabatic temperature gradient above 4 km altitude, indicating the top of the boundary layer.

The current ground-track and wind-speed analysis predicts winds of about 0.3 to 1 m s^{-1} near the surface. This velocity can be produced by any number of sources including pressure and temperature gradients and tides[10].

Migration of surface material

The acquisition of visible spectra at known locations in the images allowed correlation of the reflectance spectra with different types of terrain. The Downward-Looking Visible Spectrometer (DLVS) was an imaging spectrometer measuring light between 480 and 960 nm as it projected the image of the slit onto the ground into up to 20 spatial resolution elements for nadir angles from 10° to 50°. Spectra were collected at nominally the same azimuths as the images, though often at slightly different altitudes (on different probe rotations). Interpolation between the times at which the spectral and image data were obtained located the spectra within the images. Determination of the surface reflectivity was hindered by scattering from the haze between the camera and the surface as well as by methane absorption. Correlation of the spectra with images was therefore best performed on measurements during which the altitude changed only slightly.

The centre of the image in Fig. 11 is displayed in true colour (that is, as the human eye would see it under Titan's atmosphere) using actual spectral data from one panorama. The area between the spectra is interpolated in azimuth. The coverage with spectra is similar to that shown in Fig. 12. The orange colour is due mainly to the illumination of the surface. Scattering and absorption (which dominate in the blue) cause the perceived true colour of the surface to change from yellow to orange with decreasing altitude. Note that the passband of the cameras peaked in the near infrared (at 750 nm), and therefore the brightness variations in the images would not necessarily be seen by the human eye.

In Fig. 12 the images are correlated with the ratio of the intensity in two methane windows (827 nm/751 nm) located in the infrared part of the spectrum where scattering is minimal and the systematic variability with nadir angle can be ignored. Reddening (high 827 nm/751 nm ratio) is concentrated at the area covered with drainage

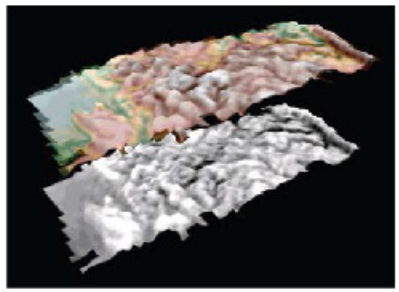

Figure 7 | Titan's surface. Perspective view of Titan's surface using a topographic model of the highland region ~5 km north of the Huygens probe landing site derived from the DISR images. The model in greyscale and false colour shows the elevation (pale white highest). The lowland plane or lakebed is to the left side of the display (in blue); the northern highlands (with the dendritic channels) is to the right.

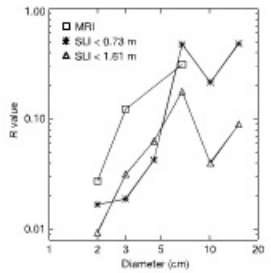

Figure 8 | Distribution of rock on the surface. Rocks larger than 1.63 cm as an *R*-plot, frequently used to describe size distribution of impact craters or crater ejecta. If *N* is the number of rocks per centimetre increment of rock size, the fraction of the surface area *A* covered by rocks with diameters between *d* and $d + \Delta d$ is approximately $N \times \Delta d \times d^2/A$. By keeping the size bin Δd proportional to the diameter *d*, the quantity $N \times d^3/A$ (the *R* value) is also proportional to the surface fraction covered by rocks of diameter *d* (with a proportionality constant of ~3). The plot shows *R* values derived from rock counts from the SLI and MRI surface images. For the SLI, *R* values from counts up to a distance from the probe of 73 cm and up to 161 cm are presented in separate curves. The comparison between the two curves suggests that the count is complete in the displayed size range. The increase of the *R* value with size corresponds to a higher fraction of the surface covered with large rocks than with smaller ones.